Nano Energy 86 (2021) 106071

Contents lists available at ScienceDirect

Nano Energy

journal homepage: http://www.elsevier.com/locate/nanoen

Full paper

Smart touchless triboelectric nanogenerator towards safeguard and 3D morphological awareness

Fang Yuan [a], Shuai Liu [a], Jianyu Zhou [a], Sheng Wang [a,b,*], Yu Wang [a,b], Shouhu Xuan [a,b,c], Xinglong Gong [a,b,c,*]

[a] CAS Key Laboratory of Mechanical Behavior and Design of Materials, Department of Modern Mechanics, CAS Center for Excellence in Complex System Mechanics, University of Science and Technology of China, Hefei, Anhui 230027, PR China
[b] Frontiers Science Center for Planetery Exploration and Emerging Technologies, University of Science and Technology of China, Hefei, Anhui 230026, PR China
[c] State Key Laboratory of Fire Science, University of Science and Technology of China, 96 Jinzhai Road, Hefei, Anhui 230026, PR China

ARTICLE INFO

Keywords:
Noncontact mode
Safeguard
Triboelectric nanogenerator
3D morphological awareness
Self-healing

ABSTRACT

The advancement of wearable smart electronics in recent years provided vital platforms for robotics, healthcare and human-machine-interfaces. Especially, as a touch-free monitoring sensor, the noncontact working mode endowed the device with superiorities of high sensitivity and favorable longer lifespan. However, the disadvantages of additional power supplies and poor mechanical property of state-of-art noncontact sensors also seriously limited their practical applications. Herein, a novel noncontact triboelectric nanogenerator (NTENG) with self-powering sensing, anti-impact and self-healing properties was developed by integrating graphene/shear-stiffening gel with shear-stiffening elastomer. Based on the electrostatic induction effect, the triboelectric self-powered behavior endowed NTENG with the capability of detecting distance and moving speed of surrounding objects without direct contact. Besides, NTENG demonstrated excellent stretchability of 90% and good self-healing mechanical-electrical properties. Furthermore, NTENG displayed safeguarding performance by efficiently dissipating 41.6% of impact force. Additionally, the NTENG-based arrays could distinguish external targets with various morphologies, and further utilize as smart sensing electric devices in walking stick, elevator button, wearable electronics in noncontact way. Besides, NTENGs could be reshaped into different 3D sensing devices structures. Due to the self-powered noncontact sensing and energy buffering characteristics, the NTENG showed favorable potentiality in wearable intelligent electronics and safeguards.

1. Introduction

The rapid flourish in artificial intelligence revolution in recent years has propelled the development of wearable electronics and functional sensors which reshapes the lifestyle of human beings. Especially, smart sensor technology is beneficial for humans and robots to perceive and understand the external world by efficiently and accurately acquiring information from surrounding environment. Recently, various developed wearable electronics with the properties of detecting complicated stimuli show vast potential application in human machine interaction (HMI) [1,2], health care [3–5] and environmental monitoring [6–8]. However, most traditional flexible sensors usually work under direct contact or deformation modes. The fatigue failure of soft polymer matrix or conductive channels of sensors under long term pressure or bending stimuli will shorten their service life. On the other hand, as the coronavirus disease 2019 (COVID-19) epidemic continues to spread around the world, an effective way to prevent infection is to avoid contact with outside objects. On these occasions, developing contactless flexible sensors has an important impact on improving the comprehensive performance of flexible sensors and fighting against COVID-19 epidemic.

So far, various noncontact sensors, based on magnetic, optical, humid, capacitive changes have been developed to avoid mechanical loadings and virus transmission [2,9–11]. However, additional power sources were always supplied to actuate these electronics. Thus, novel self-powered sensors based on triboelectric nanogenerators (TENGs) [12,13] with the ability of actively harvesting mechanical energy from ambient environment and generating electrical signal itself showed high potential to address this issue. Based on such devices, the self-powered

* Corresponding authors at: CAS Key Laboratory of Mechanical Behavior and Design of Materials, Department of Modern Mechanics, CAS Center for Excellence in Complex System Mechanics, University of Science and Technology of China, Hefei, Anhui 230027, PR China
E-mail addresses: wsh160@ustc.edu.cn (S. Wang), gongxl@ustc.edu.cn (X. Gong).

https://doi.org/10.1016/j.nanoen.2021.106071
Received 17 February 2021; Received in revised form 10 April 2021; Accepted 10 April 2021
Available online 15 April 2021

sensors could actively generate electrical signal in response to the trigger from ambient environment without the necessity for driving power [14]. Fortunately, some recently invented TENGs were developed to work under noncontact operating mode [15,16]. For example, a novel noncontact screen sensor was developed by using monolayer grapheme/polyethyleneterephthalate substrate and it could recognize multi-gestures [17]. Thus, the novel touch-free recognition technology not only fills in the technical gap in intelligent HMI, but may generate a new surge of innovation in the operation modes of flexible sensing devices [18].

Wearable electronics with noncontact working mode could effectively avoid the mechanical failure and show longer lifespan. However, the actual working environment of self-powered sensors were always complex and unpredictable. For example, collision and impact forces are also widespread in daily life which may lead to sensor failure and human injury. Therefore, it is of great practical value to develop multifunctional noncontact sensors with enhanced mechanical properties by choosing smart polymer matrix with self-healing and anti-impact properties. Shear stiffening gel (SSG) [19], as a viscoelastic polymer whose modulus could drastically increase under high strain rate loading, could change its state from liquid to solid. Thus, it showed promising application in damper and safeguards [20]. Recent reported SSG-based e-skins [21], possessed good electrical sensitivity and ideal anti-impact performance which could reduce the impact force by nearly 50%. Based on the self-healing and impact-buffering capabilities, SSG-based TENGs may be endowed with the possibility to simultaneously maintain the self-powered performance for noncontact sensing electronics and anti-impact effect for safeguard. Regrettably, such an attempt has not been conducted so far.

Herein, a self-powered sandwiched noncontact triboelectric nanogenerator (NTENG) integrated by graphene/SSG electrode and SSE shell based on electrostatic induction and triboelectric effects was presented. The self-powered behavior ensured NTENG capable of detecting distance and moving speed of moving objects. Besides, the NTENG could dissipate 41.6% of the impact force. More interestingly, the NTENG units with self-healing property could not only integrate into linear and planar arrays, but also further assemble into 3D triangular pyramid or cubic structure. These sensor arrays could be utilized as smart noncontact electric devices in walking stick, elevator button, wearable electronics for perceiving environmental variations. In addition, the self-assembled 3D NTENG was capable of adhering on complex surfaces to detect the azimuth information and motion state of potential dangerous moving objects. Thus, the as-designed NTENG show favorable applications in HMI, 3D structural measurement, healthcare and safeguard.

2. Material and methods

2.1. Materials

Hydroxyl silicone oil and boric acid were purchased from Sinopharm Chemical Reagent Co. Ltd, Shanghai, China. The methly vinyl silicone rubber (VMQ 110–2) and few-layer graphenes were bought from Shenzhen Muwei Technology Co., Ltd. and Shenzhen Siheng Technology Co., Ltd, China. All chemical reagents were of analytical purity and used as received without further purification.

2.2. Fabrication of NTENG

Hydroxyl silicone oil and boric acid with a weight ratio of 20: 1 and varying amounts of graphene were vigorously stirred to yield a homogeneous mixture. After heating in a 180 ℃ oven for 90 min, a few drops of octanoic acid were added. Then, the mixture was stirred and heated at 180 ℃ for another 30 min. After cooling to room temperature, the mixture was homogenized by the two-roll mill (Taihu Rubber Machinery Inc., China, model XK-160). Next, SSG and VMQ were mixed together in a double-roll mill. Benzoyl peroxide was added as the vulcanized agent at 4.0 wt% and the rubber mixture was cured at 90 °C under 20 MPa for 15 min. Finally, the NTENG was developed by integrating graphene/SSG with SSE.

2.3. Characterization

The morphology of graphene and c-SSG was characterized by field emission scanning electron microscopy (FE-SEM, XL30 ESEM). The static approaching-separating experiment was conducted on an electroforce dynamic system (TA ElectroForce 3220, TA Instruments) and a micro/nanomechanical testing system (FTMTA02, Femto Tools, Switzerland). The dynamic impact test was performed using a drop hammer test device (ZCJ1302-A, MTS System Co., America) equipped with accelerator and force sensors and a data acquisition system. The electric signals of NTENG arrays were acquired by low-velocity impact drop tower testing system consisted of a drop tower test device (ZCJ1302-A, MTS Co. Ltd, China), an acceleration sensor, force sensors, and a dynamic signal test and analysis system (DH5920N, Donghua Testing Technology Co., Ltd, Jiangsu, China).

3. Results and discussion

3.1. Structures and working mechanism of the NTENG

The NTENG was developed by integrating conductive shear stiffening gel (c-SSG) with shear stiffening elastomer (SSE), the corresponding morphologies were displayed in Fig. S1. Derived from the visco-elastic properties of SSG, the flexible self-powered NTENG (Fig. 1a) exhibited mechanical self-healing as well as energy dissipation performance. The mechano-electrical mechanism of NTENGs was presented in Fig. 1. Generally, dynamic B-O cross bonds with p orbital of B atoms and electrons of O atoms were formed in SSG with rate-dependent mechanical characteristics (Fig. 1b) [19]. Furthermore, the instantaneous self-healing capability of the c-SSG and SSE was also attributed to the cross bonds in the polymer matrix (Fig. 1b). Besides, parts of the unreacted OH groups could form dynamic hydrogen bonds which also result in the self-healing properties of SSG [22,23]. These dynamic bonds, cleaved upon damage, could be cured during the healing process without any external stimuli. Thus, NTENG units could be assembled into linear and planar arrays which showed high adaptability (Fig. 1a).

In general, contact electrification process was firstly conducted to electrify fluorinated ethylene propylene (FEP) film. Then, the movement of FEP could lead to spatial electrostatic inductions with dynamic noncontacting sensing properties [18]. The detailed working mechanism was schematically demonstrated in Fig. 1c. In the initial state, FEP film and NTENG were separated away (Fig. 1c-i). Once FEP began to approach the NTENG surface, more positive charges would be accumulated on the c-SSG electrode to balance the negative charges on FEP. Thus, free electrons flowed from the c-SSG to the ground, generating an output current signal (Fig. 1c-ii). Conversely, when FEP gradually moved away, the c-SSG would attract electrons to neutralize the positive charges on its surface, generating a reversed output current signal (Fig. 1c-iii). When the FEP returned to its original position, a full cycle of the electric signal generation process was completed. The transferred charges were calculated by integrating the current-time curve (Fig. 1c-iv), the calculated electric charges transferred during approaching process (0.714 nC) were slightly higher than charges transferred during separating process (0.634 nC). To verify this proposed mechanism, the corresponding potential distributions under the open-circuit condition were simulated by the COMSOL software (Fig. 1c-v). A theoretical model was simultaneously built to elucidate the effects. The electric potential φ of the electrode imposed by a surface charge of the moving object was set as [24].

$$\varphi = -\iint \frac{\sigma}{4\pi\varepsilon} \frac{1}{\sqrt{x^2+y^2+z^2}} dxdy \quad (1)$$

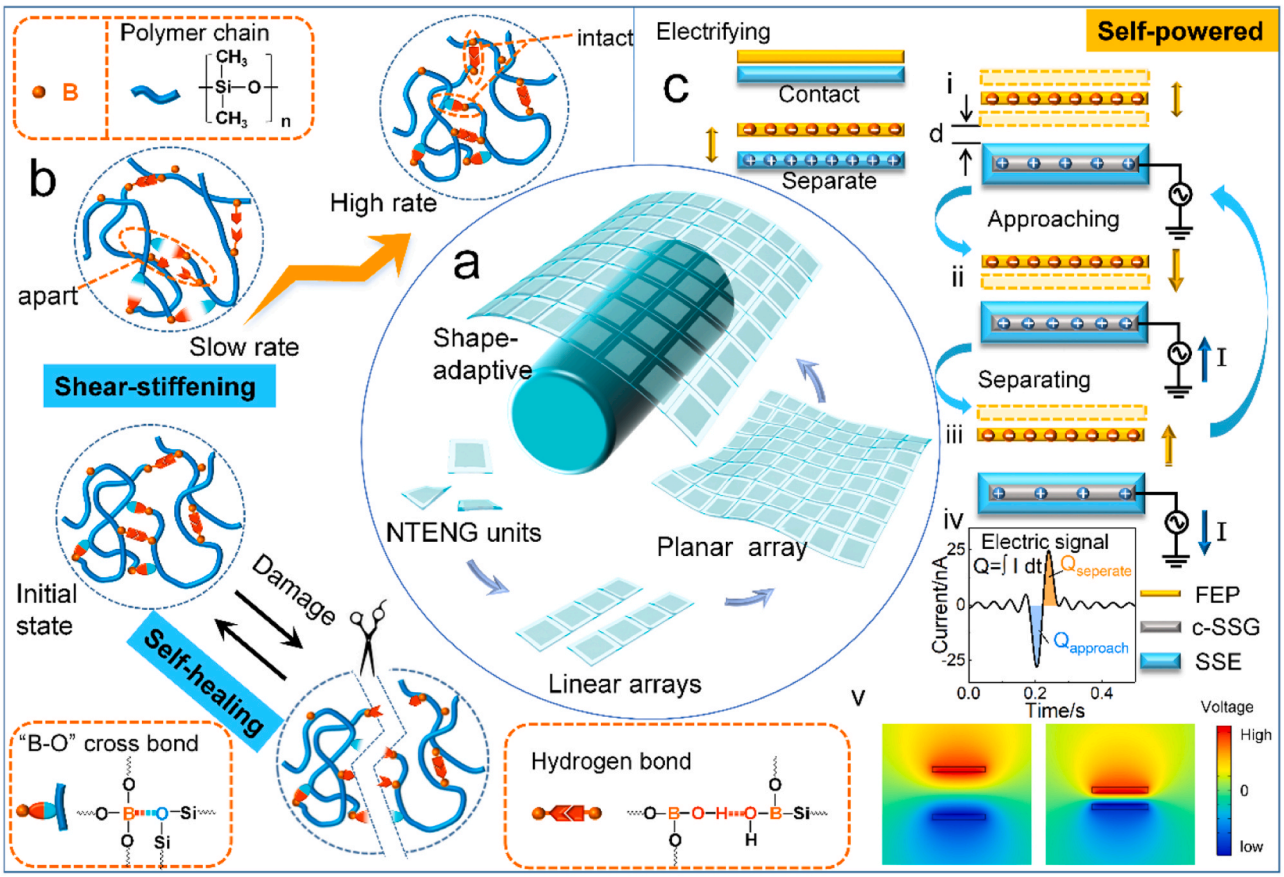

Fig. 1. (a) High adaptability of the assembled NTENGs and working mechanisms of (b) protective, self-healing and (c) self-powered properties.

σ was the charge density among FEP surface, ε was vacuum dielectric constant. The charges distribution were considered to be uniform in y-direction. a, b were the length of x, y-axis, respectively. Eq. (1) could be simplified as

$$\varphi = -\frac{b\sigma}{4\pi\varepsilon} ln\frac{\sqrt{a^2+z^2}+a}{\sqrt{a^2+z^2}-a} = -\frac{b\sigma}{4\pi\varepsilon} ln\left(1+\frac{2a}{\sqrt{a^2+z^2}-a}\right), z = z_0 + z(t) \tag{2}$$

The matched load of an oscilloscope was 1 MΩ, which was nearly five orders of magnitude higher than the sheet resistance of c-SSG electrode. The voltage flew in the circuit was mostly distributed in the oscilloscope. Therefore, voltages recorded by the oscilloscope could be considered as open circuit voltages generated within the electrodes.

3.2. *Noncontact sensing performance of NTENG*

FEP film as an active layer was vertically reciprocated with different frequencies at different starting points above the NTENG unit in noncontact mode by an electroforce dynamic system (Fig. 2a). Before the measurement, an additional SSE was used to rub and charge the FEP film. The electric charges on the FEP film was determined to be about −21.6 nC by the integral area of the corresponding I-t curve (Fig. S2). The peak value of output voltage varied with loading distance of 0.1–8 cm from 83.2 to 0.53 mV (Fig. 2b, Fig. S3). Besides, the relationship between the voltage data and minimum distance in Fig. 2b was fitted well by Eq. (2). And the curve of the voltage-distance around 1 cm was linear fitted with slope of -1.56 mV/mm (Fig. 2c). Fig. 2d, e presented the output voltage and transferred charge of the NTENG at different distances from 0.5 to 3 cm, respectively. With the increase of the minimum distance between the NTENG and FEP film, all these electric outputs decreased. For example, as the minimum distance increased from 0.5 to 3 cm, the average peak voltages decreased from 32.4 to 3.24 mV, while the currents decreased from 32.4 to 3.24 nA. Correspondingly, the transferred charge in one cycle decreased from 0.71 to 0.072 nC. Notably, to more accurately evaluate the distance sensitivity of the NTENG, the increment of the minimum distance were set as 0.125, 0.25, 0.75, 1 mm to acquire the vertical distance resolution. As shown in Fig. S4, the voltage signals remained unchanged until the minimum distance increased to 1.175 cm which demonstrated that the vertical distance sensitivity of NTENG was 0.75 mm (with the distance around 1.1 cm). Fig. 2f, g exhibited the electric outputs of the NTENG with the moving frequency of 2–20 Hz when keeping the minimum distance at 1 cm. It revealed the voltage and current increased as the moving frequency increased. At 20 Hz, the output voltage and current reached 32.3 mV and 32.3 nA, respectively. The amount of transferred charges decreased slightly from 0.63 to 0.49 nC with the reduction of frequency. This result revealed the amount of transferred charge was mainly related to the distance between NTENG and FEP which guaranteed the reliability of NTENG for distance detection. Furthermore, the applied displacement waveform of FEP film also had a dramatic influence on the output performance of NTENG. Interestingly, the voltages response varied with different square, triangular and block loading waves (Fig. S5a). The sensing behavior of NTENG with frequencies from 1 to 20 Hz under square and triangular waves were also studied in Fig. S5. In addition to the vertical approaching-seperating mode, the NTENG could also output voltage under sliding approaching-seperating mode (Fig. S6). This result proved the as designed NTENG could sense various stimuli in non-contact mode.

The self-powered sensing performance of NTENG under different elongations was evaluated to mimic its practical working conditions. Originated from the favorable visco-elasticity of SSE, NTENG could stably maintain its shape even under large deformation (Fig. 2h). The

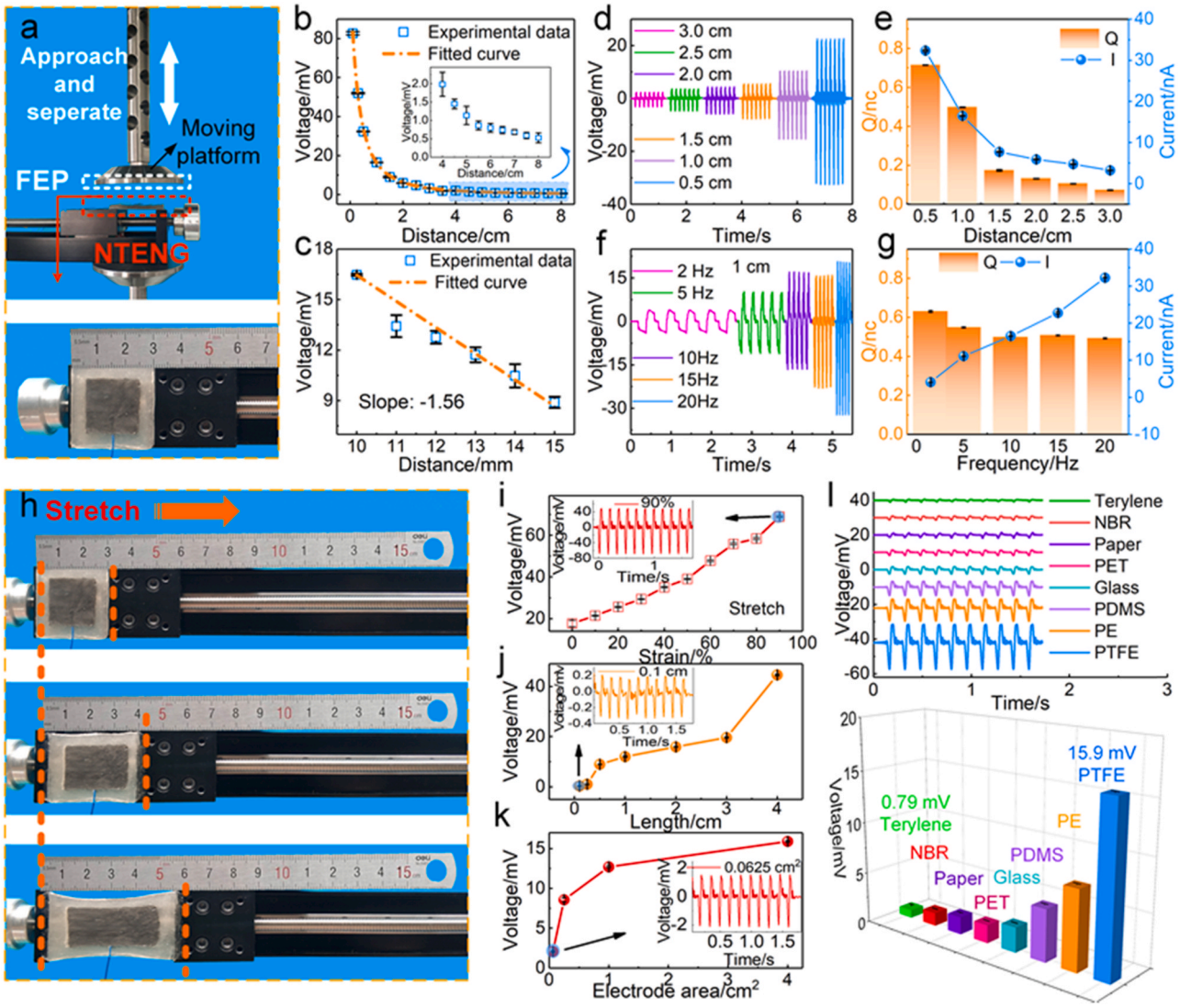

Fig. 2. Noncontact sensing performance of NTENG in vertical mode. (a) Photographs of the test platform, (b, c) voltages under different minimum distances and sensitivity around 1 cm. (d, e) the loading distance (0.5–3 cm) and (f, g) frequency (2–20 Hz) dependent voltage, current and transferred charge of NTENG. (h) The stretched NTENG with sliding table and (i) the corresponding output voltages. Output voltages varied with the sizes of (j) the electrified layer of FEP film and (k) c-SSG electrode. (l) The electric responses with various materials of electrified layer.

vertical loading condition was uniformly set as: the minimum distance between the NTENG and samples was 1 cm; the traveling range was set as reciprocating 1–2 cm away from the NTENG; and the moving frequency was set as approaching and separating in a speed of 175 mm/s with an interval of 0.1 s. The induced voltages were very stable during cycles of approaching-separating processes from 17.7 to 68.9 mV with strain increasing from 0% to 90% (Fig. 2i). Besides, the resolution of NTENG as a noncontact sensor was investigated (Fig. 2j, k). Keeping the sizes of NTENG and inside c-SSG at 3×3 cm^2 and 2×2 cm^2 respectively, the voltages increased from 0.322 to 44.6 mV as the sizes of the FEP film varied from 0.1×0.1–4×4 cm^2 (Fig. 2j). And the responsive output voltage was also stable even FEP film was cut to 0.1×0.1 cm^2. Simultaneously, when FEP was 2×2 cm^2, the output voltages increased from 2.08 to 15.9 mV with the increase of the electrode sizes from 0.25×0.25–2×2 cm^2 (Fig. 2k). Furthermore, the NTENG could also detect different approaching materials according to various voltage signals (Fig. 2l, Fig. S7). In addition, the output performance of NTENG under different temperatures and humidities were simultaneously explored (Fig. S8). The results showed that the output voltage of NTENG not only kept stable when temperature and humidity varied from 273 to 337 K, 40–98%RH, but also barely changed even after 40 min (Fig. S9). Thus, the as-designed NTENG with self-healing effect, high resolution and excellent reliability showed potential application as a noncontact self-powered sensor.

Self-healed devices could autonomically restore a rupture as unexpected destruction occurs, which could efficiently prolong their life span [25,26]. The mechanical healing performance of SSE was assessed by tensile tests and the healing efficiency was quantitatively calculated by the recovery of fracture strain [27–29]. As shown in Fig. S10, with a healing time of 180 min, mechanical healing efficiency reached about 90% at ambient conditions. Due to the plastic and adhesive characteristic of SSG, the as-designed SSE and NTENG exhibited good self-healing characteristics at ambient conditions. NTENG was firstly cut into two pieces. After contact, the crack could heal autonomously within 1 min (Fig. 3a). The two severed pieces of NTENG could be readily stretched again after being gently contacted. At the stretch of 30%, the output voltage, current and the amount of transferred charges of the healed NTENG were 26.8 mV, 26.8 nA, 0.58 nC, respectively (Fig. 3b, c). Compared with 29.4 mV of the original NTENG under 30% stretch before healing process (Fig. 2i), the degradation in self-powered sensing property was slight. Besides, NTENG during the cutting and self-healing process also showed interesting electric performance (Fig. 3d, e). Firstly,

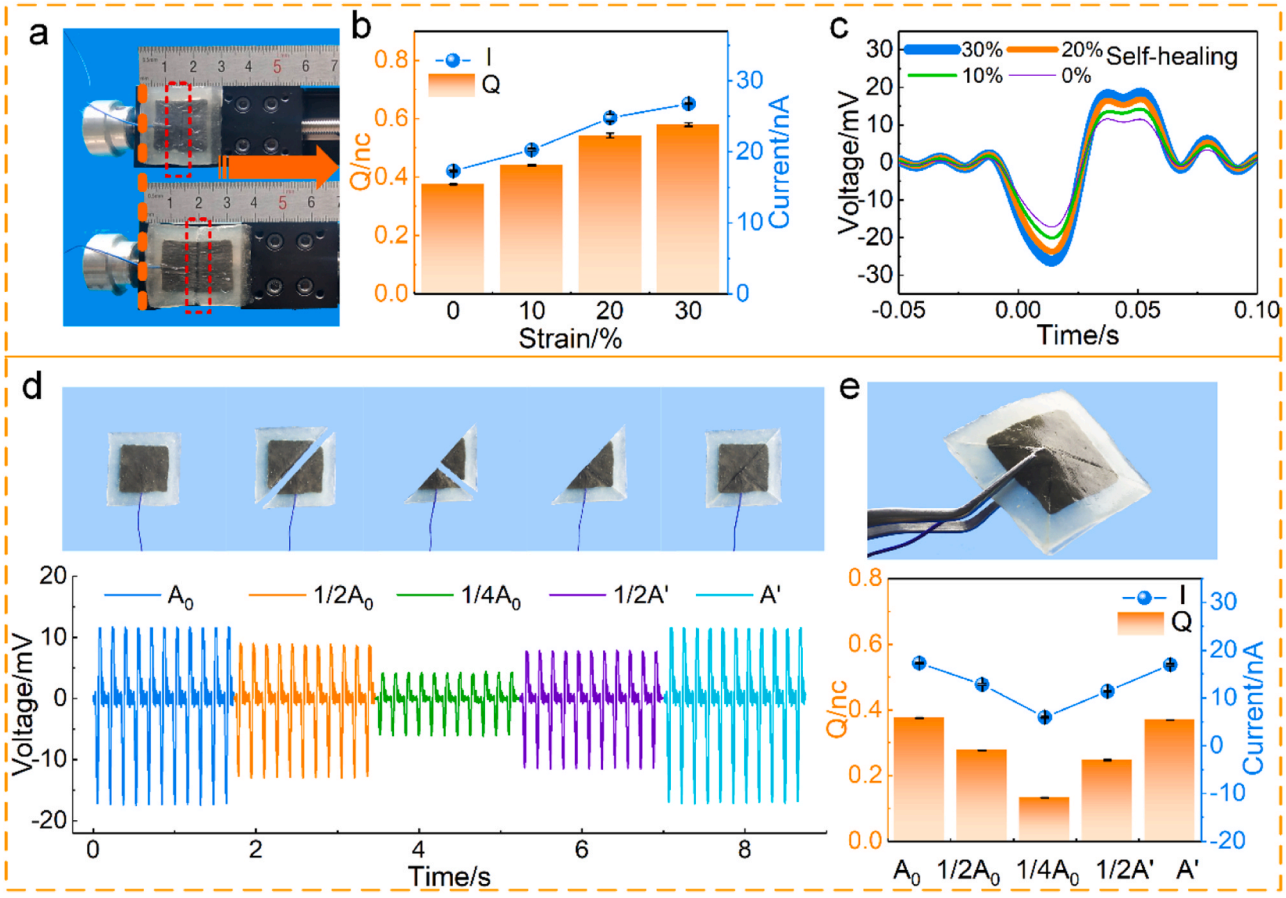

Fig. 3. The electric self-healing performance in noncontact mode. (a) The healed NTENG under stretch on the sliding table and (b, c) the corresponding sensing current, transferred charge and voltage of NTENG. (d, e) The digital photos of the cut and healed unit and the corresponding electrical performance in noncontact way.

the voltage and transferred charges were reduced from 17.3 mV and 0.38 nC to 12.8 mV and 0.28 nC as half NTENG was cut, respectively. And the voltage signal kept decreasing to 6 mV when only quarter NTENG remained. However, the signal recovered to 11.4 mV as two quarters healed and finally recovered to 17 mV when the other half NTENG got in touch. These results suggested NTENG exhibited a good electrical self-healing property which was attributed to the highly mobile polymer chains, dense hydrogen and cross bonds of SSG composites.

To further explore the sensing response of NTENG under different loading velocities, an impactor stick with FEP film was dropped from different heights, and a hinder was set to stop the dropping impactor at 1 cm above the NTENG (Fig. 4a). When the drop height increased from 1 cm to 150 cm, the approaching velocities were increased from 0.443 to 5.42 m/s and the corresponding peak induced voltage values varied from −38.6 to −489 mV (Fig. 4b). Notably, both voltages and the transferred charges apparently linearly increased in the height of was 5–11 cm. Voltage-time curves with drop height of 5, 10, 30, 60, 100, 150 cm were displayed in Fig. 4c. Interestingly, time derivative of voltage signal was closely related to the accelerometer signal. As shown in Fig. 4d, when the voltage reached minimum of −281 mV, the acceleration and time differential of voltage (dV/dt) started to increase with falling height of 9 cm. The detailed acceleration (dv/dt)-t and dV/dt-t curve curves were displayed in Fig. 4e, the two curves showed a similar trend with time. To further study the relationship between the acceleration and dV/dt, the peak values of dV/dt under various approaching accelerations were fitted. As shown in Fig. 4f, for a relatively small range of accelerations (between 0 and 0.88 km·s^{-2}), the result showed a positive linear relationship with a correlation coefficient (R^2) of 0.94 and slope of about 0.24. The slope kept decreasing to 0.09 and 0.035 in the ranges 0.88–0.25 km·s^{-2}, and 0.25–0.47 km·s^{-2} with R^2 of 0.96 and 0.97, respectively. The time differential of voltage (dV/dt) was obtained according to Eq. (2).

$$\frac{dV}{dt}=\frac{d\varphi}{dt}=\frac{d\varphi}{dz}\frac{dz}{dt}=\frac{b\sigma}{2\pi\varepsilon}\frac{a}{z}\frac{1}{\sqrt{a^2+z^2}}\frac{dz}{dt},\frac{dz}{dt}=\frac{\partial z}{\partial v}\frac{dv}{dt}+\frac{\partial z}{\partial t} \tag{3}$$

When applied loadings with lower speeds, an approximately linear relationship could be obtained from Eq. (3) between dV/dt and acceleration, which was close to the experimental results. However, upon further increasing the speed, the charge density (σ) on FEP surfaces might be decayed because of the increasing of air friction [30]. Thus, the slope of the fitted curve was decreased when the impact speeds were higher.

Derived from the shear stiffening effect of SSG, NTENG showed the ability of dissipating and absorbing impact energy. To simulate the unexpected impact forces from the environment, impact loading tests on NTENG were systematically performed by using drop hammer machine without the hinder (Fig. 4g). NTENG was fixed on the force transducer, which was further placed on the bottom of a metal pedestal. As a comparison, the pure VMQ specimen (the same size as NTENG) and metal pedestal without specimens were both tested. During the impact, the force signals were captured and recorded using an oscilloscope. Falling height dependent impact forces of force sensor, VMQ and NTENG were presented in Fig. 4h. After the impact from 1.5 m, VMQ was damaged with cracks. However, the soft NTENG was only deformed with a shallow, indicating better anti-impact performance (Fig. 4g). After introducing VMQ, the impact forces were decreased when compared with those directly loaded on force sensor. For example, keeping the height at 60 cm, the maximum force (2577 N) after absorbing by VMQ

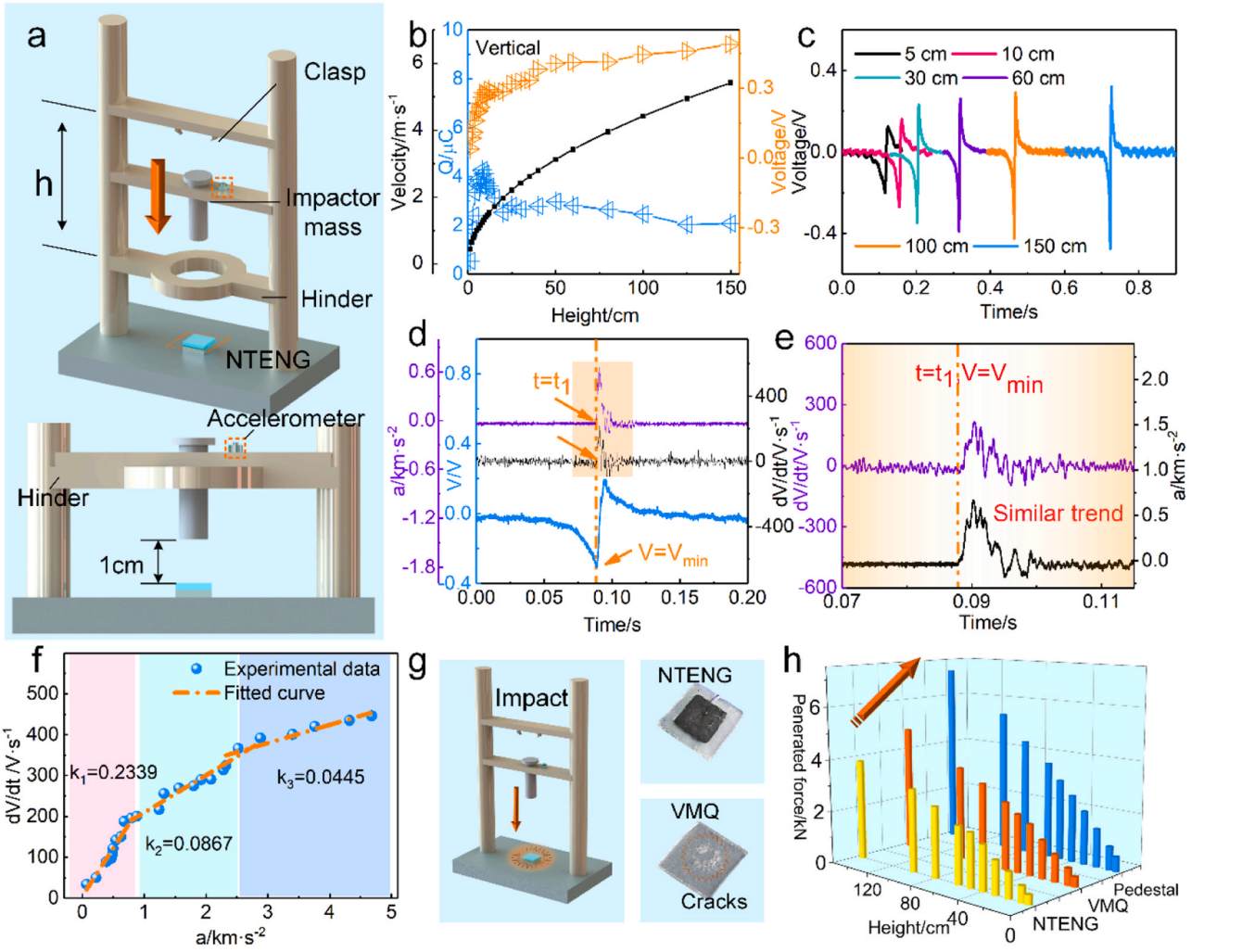

Fig. 4. Electric and mechanic performance under impact by (a) drop hammer machine system. (b) The voltage, transferred charge and approaching velocity with the drop heights from 1 to 150 cm and (c) some typical voltage-time curves. (d) Acceleration curve of drop hammer from 9 cm, the corresponding induced voltage and its time differential (dV/dt) curves with time; (e) detailed comparison of the acceleration-t and dV/dt-t curve. (f) Peak values of dV/dt under different approaching accelerations and the slopes were linear fitting. (g, h) Impact energy dissipation performance of NTENG, VMQ and metal pedestal with impactor dropping from 1 to 150 cm when the hinder of drop hammer machine was removed.

was 3689 N on pedestal. This indicated VMQ was capable of buffering the impact force. More importantly, the peak force of the NTENG was 2156 N, further reducing to 58.44%. Clearly, NTENG showed the best energy adsorption properties. In conclusion, as a wearable velocity sensor, the NTENG could not only detect the moving object before contacting, but also provide protection even if the impact accidentally loaded on people.

3.3. Self-powered sensing properties to 3D surfaces by noncontact modes

Owing to the self-healing properties of the polymer composites, NTENG units could be facilely assembled into large sensor array. Firstly, a linear 4 × 1 array was fabricated by integrating four NTENG units (2 × 2 cm^2). When the array slid above (1 cm) a plane decorated with distributing blockages (Fig. 5a), the third and fourth channel outputted induced voltages of 2.07 and 2.61 mV at first, indicating only "3, 4" sensor units sensing blockages (Fig. 5b). Furthermore, in the last triggered period, four channels outputted voltages of 1.42, 2.5, 5.34, 10.4 mV, respectively. It indicated that the array passed 4 blockages with different heights on the panel. Hence, an electric mapping was acquired (Fig. 5c) which successfully matched with the monitored target. This suggested NTENG array could sense and detect the distribution and concave-convex degree of 3D surface by sliding approaching mode without contact. Thus, an 8 × 8 matrix (Fig. 5d) with size of 6 × 6 cm^2 was further developed to detect various 3D structures in vertical approaching mode. As the moulds vertically approached to the array, different induced voltages were generated owing to the different distances between array and moulds with circle plane, convex, concave and helix structures (Fig. 5e–h). The electric mappings could ideally reveal the morphologies of uniform cake, ring, spot and helix moulds respectively and the voltage signals were displayed in Fig. S11. In conclusion, this NTENG array with ideally mapping sensing properties showed potential in 3D structure measurement.

3.4. Applications of NTENG as flexible smart touchless electronics

Touchless sensing was critically important in artificial intelligent systems, remote safety, and healthcare monitoring [11,31]. The as-designed NTENG exhibited stretchable, self-healing and shape-adaptive properties. Thus, it could be attached to the uneven surfaces as a touchless sensor to monitor external environment. Three NTENG units were bonded with each other as a linear sensor array and adhered to a walking stick (Fig. 6a) to help people move forward in darkness. Three units could detect left, forward, and right directions.

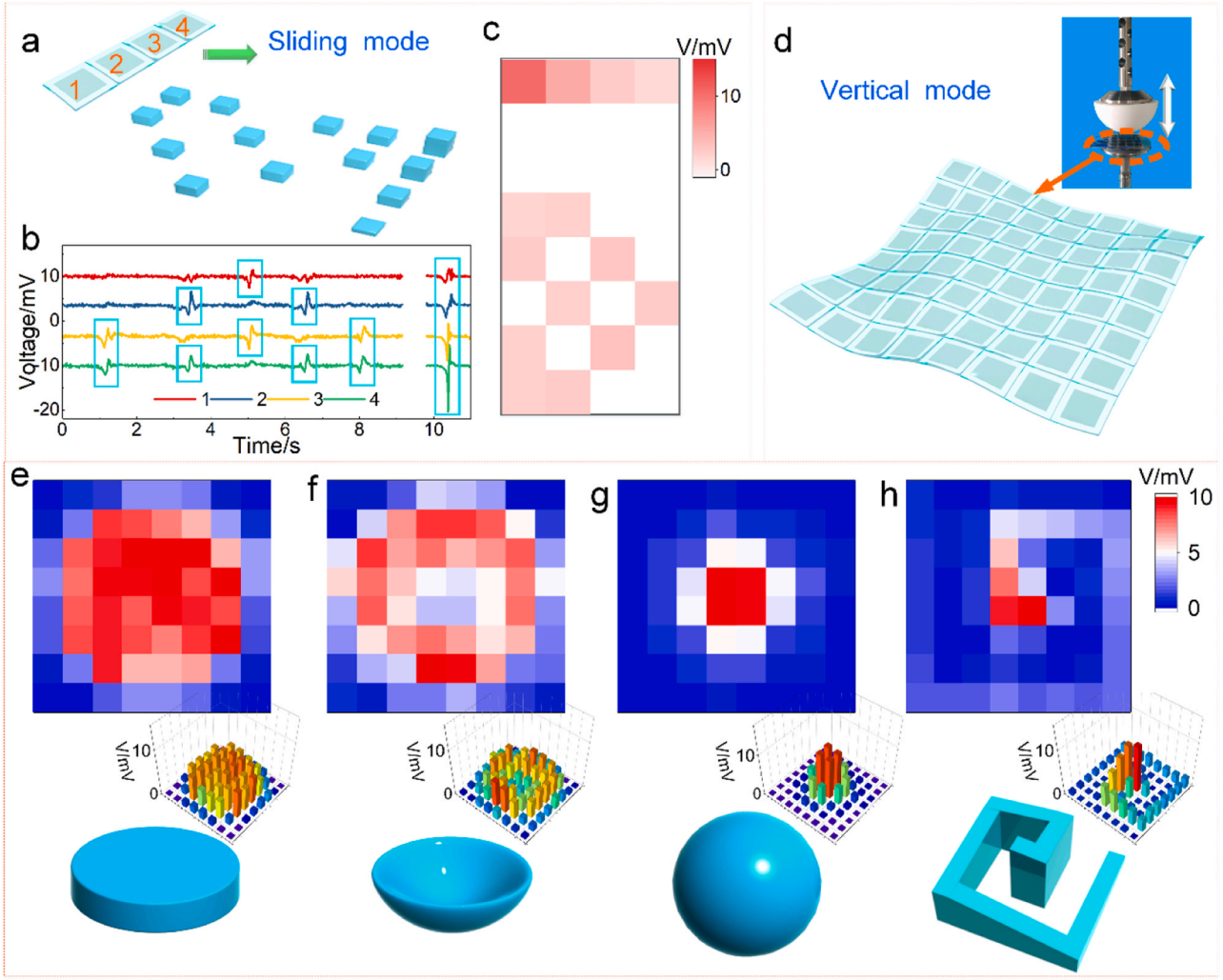

Fig. 5. Self-powered sensing performance of NTENG array to 3D complicated structures. (a–c) Detecting complex pattern by 4 × 1 array in sliding noncontact mode. (d–h) Electric responses to plane, concave, convex, helix surfaces with voltage mappings in vertical noncontact mode.

The stick with NTENG generated electric signals when it was close to obstacles and the signals could give guidance for the users. When human walked into dark corridor, the stick could be used to explore the road. In the 1 and 2 stages (Fig. 6b), voltage signals, generated by the medium and left NTENG units (Fig. 6c), indicated obstacles appeared in the front and left directions which could not pass in these directions. Then, the user turned right and kept moving on to simultaneously explore the road ahead by the stick. In the 3 stage, the left unit still generated electric signals as the stick explored the left hallway during moving ahead. When voltage pulses were outputted by the medium unit, this meant the left and the forward road could not pass, so the user stopped moving forward and turned right (4 stage in Fig. 6b). At this period, the user walked in the same way. When the stick did not generate obvious pulse signals, the user finally left from the complicated environment (5 stage). The results demonstrated the flexible NTENGs could be attached to uneven objects to help people avoid dangerous obstacles before touching them.

With the current COVID-19 pandemic, contactless sensing-actuation technology was quite important for epidemic prevention and health care. Therefore, the as-designed NTENG could work as a noncontact self-powered sensor to detect human stimuli. For example, NTENG showed potential as elevator buttons to sense the number of floor levels which people did not need direct contact. NTENGs could be easily integrated into flexible 3 × 3 matrix. Nine NTENG units with a protective cover represented various floors from 1 to 9 (Figs. 6d and S12). As the fingertip approached the “5”, this channel generated 3.04 mV pulse voltage and the corresponding signals distribution displayed in Fig. 6e. This indicated people wanted to go to fifth floor. Besides, Fig. 6d, e also illustrated when two fingertips simultaneously approached different NTENG buttons of “3” and “5”, two pulse signals were generated by these channels. Fig. 6f also displayed the simulated location and magnitudes of generated voltage signals of one- and two-nontouch modes by COMSOL software. Besides, the NTENG array could also act as a wearable self-powered electronic device to monitor human movements in noncontact mode. For instance, the real-time moving routes of human hands was identified by measuring the output signal of every single pixel (Fig. 6g). When writing “C”, “Z” and “S”, they could be recognized based on the voltages of NTENG array (Figs. 6h–j and S13). Furthermore, all pixels were connected with the LEDs and a multi-channel dynamic charge amplifier, the trajectory of fingertip was optically demonstrated by luminescent LEDs in the same trajectory of “+” (Movie S1). In short, the proposed NTENG was proven to be potentially effective in daily healthcare and HMI.

3.5. *Self-assembling and spatial sensing performance of NTENGs*

To further demonstrate the self-healing and self-assembling properties, two-dimensional (2D) NTENG units could be developed by moulds and were bonded with each other and reassembled onto three-dimensional (3D) surfaces. Four planar 2D triangle NTENG units turned into 3D triangular pyramid (Fig. 7a). Besides, planar NTENGs

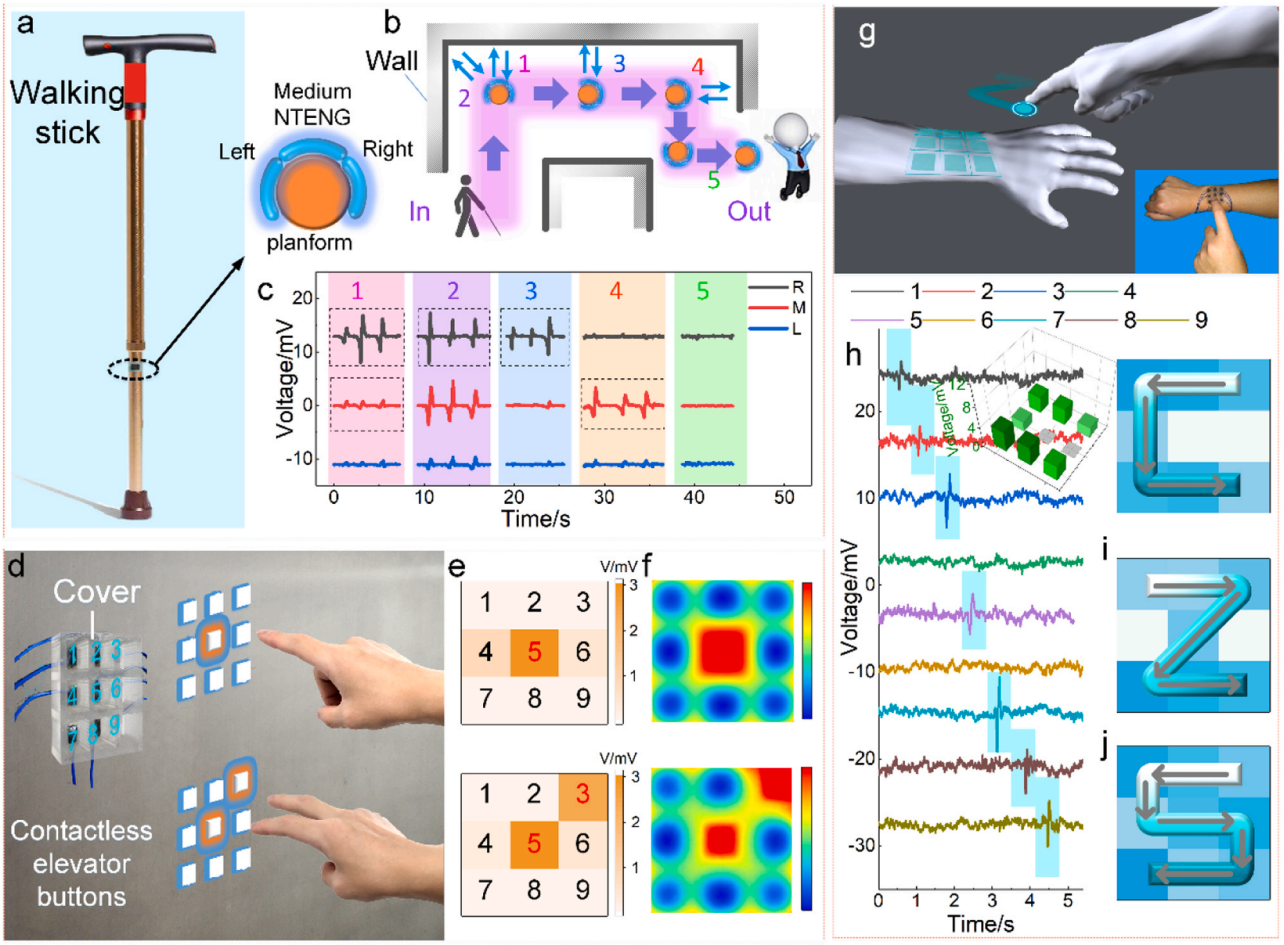

Fig. 6. The applications of NTENG. (a–c) The noncontact sensing performance of NTENGs when adhered on a walking stick to help the user to move in dark channel. (d–f) NTENG array worked as noncontact self-powered elevator button sensors, the corresponding signal mappings of NTENG array could show external human stimuli. (g-j) The soft NTENG array adapted to the wrist to detect human movements in noncontact way.

were folded and automatically healed the junction lines to form a 3D cube (Fig. 7b). This indicated NTENGs could be easily reshaped into arbitrary, complicated 3D arrays. Besides, 3D printing technology could also be used to develop the 3D arrays and they presented similar electrical performance, indicating its potential for large-scale production (Fig. S14). In addition, the output voltage signals generated by five surfaces were measured by multi-channel dynamic signal test system when moving object passed through different azimuths (Fig. 7c, d). As the moving object horizontally went by the above surface (B) of the cube from the point (1, −1, 3) to point (1, 1, 3) (Fig. 7c-i), the output voltage by channel B was 32.71 mV which was obviously much higher than the signals from other channels. Besides, as the moving object slantly went by the junction line between surfaces B and C (Fig. 7c-ii), channels B and C could generate dramatic voltage signals. Besides, three channels outputted voltages when moving object passed through the vertex of three surfaces (Fig. 7c-iii). The NTENG could not only be capable of sensing the orientation of the passing object, but also detect the speed of the moving object. As shown in Fig. 7e, the waveforms of output voltages varied with different speeds. The waveforms of voltage signals were gentle and flat as a slow moving object passed by the junction line between B and C of cubic NTENGs. And a wide pulse voltage was generated in real-time with the pulse width of 0.823 s and peak voltage of 28 mV. On the contrary, the waveforms were sharpen and narrow as a object swiftly passing by, the duration time was 0.235 s (shorter than lower speed). Therefore, the rapid or slow movement could be determined by the change rate of voltage signals. In conclusion, the self-healing and self-assembled performance enabled the NTENGs to turn into 3D structure and fit on complex surfaces to detect the azimuth information and motion state of potential dangerous moving objects in complex environment.

4. Conclusion

In this work, a flexible NTENG with noncontact self-powered sensing, self-healing and anti-impact performance was developed by integrating SSE with graphene/SSG composites. NTENG could detect the distance and speeds of moving objects based on electrostatic induction and triboelectric effects. The flexible NTENG could output a stable voltage of 68.9 mV even under stretch to 90% during approaching-separating process. Based on the shear stiffening effect, NTENG could impede and absorb 41.6% of external kinetic energy during accidental impact loading. Besides, NTENGs showed good electro-mechanic self-healing properties and could be assembled into various 3D structures. NTENG based arrays could sense and detect various morphologies in noncontact way. Based on the self-powered noncontact sensing characteristic, the array sensor could utilize as smart electric devices in walking stick, elevator button, wearable electronics for sensing external variations. The self-assembled cubic sensor could not only achieve 3D position sensing, but also detect the moving speed of the object passed by. In conclusion, the soft triboelectric NTENG with self-powered noncontact sensing property exhibited great potentiality in intelligent devices for darkness, toxic or harmful environments and human-machine interfaces.

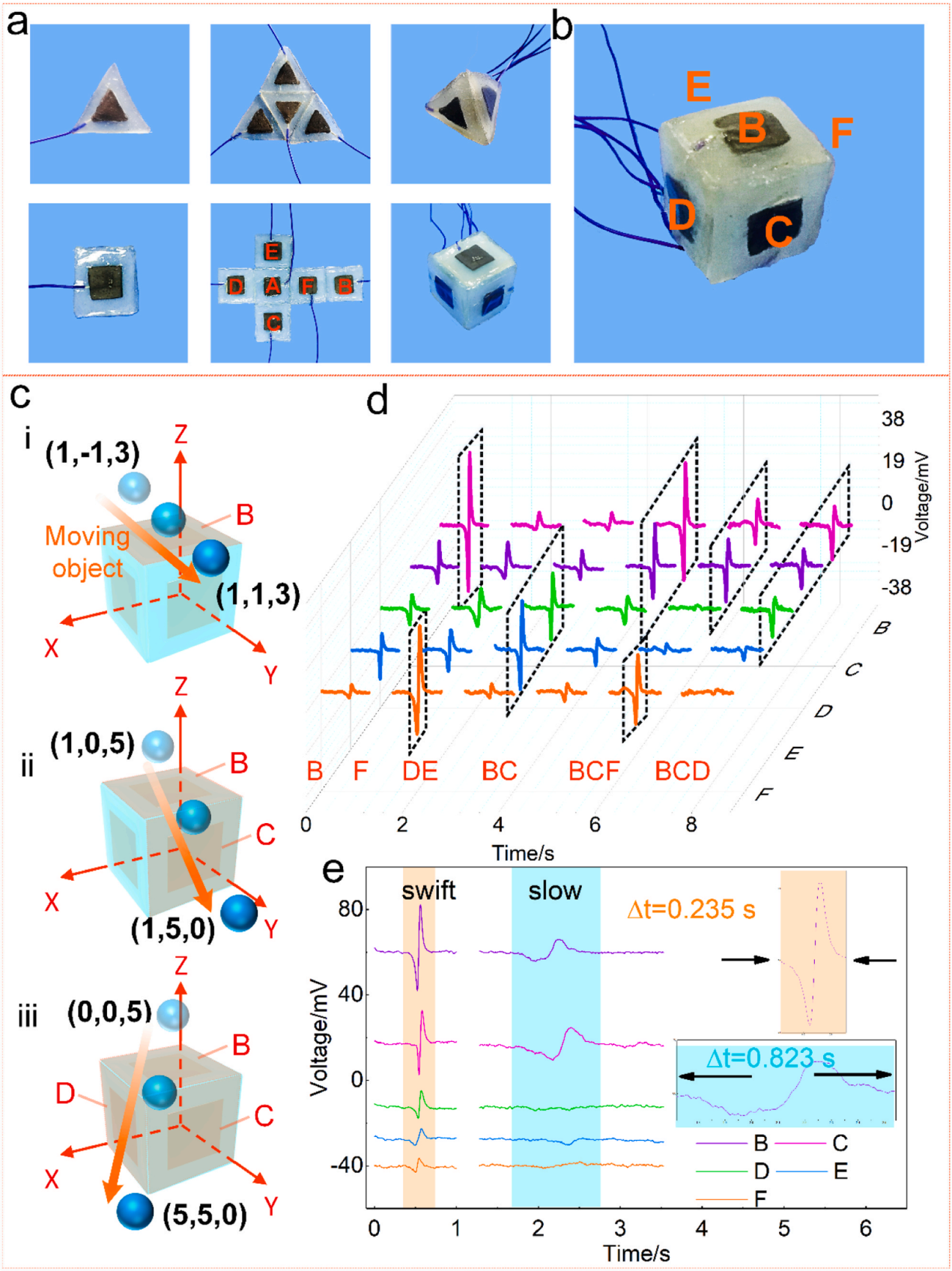

Fig. 7. Self-assembling and spatial sensing performance of NTENGs. (a) The self-assembling performance of NTENGs from 2D to 3D structures. (b) Cubic NTENGs as a 3D noncontact sensor to detect (c–e) the location and speed of passing objects.

CRediT authorship contribution statement

Fang Yuan: Investigation, Writing - original draft, Methodology, Visualization. **Shuai Liu**: Investigation, Computational simulation. **Jianyu Zhou**: Investigation, Data curation. **Shouhu Xuan**: Formal analysis, Conceptualization. **Yu Wang**: Software, Data curation. **Sheng Wang**: Formal analysis, Writing - review & editing. **Xinglong Gong**: Resources, Supervision, Project administration, Funding acquisition.

Declaration of Competing Interest

The authors declare that they have no known competing financial interests or personal relationships that could have appeared to influence the work reported in this paper.

Acknowledgments

Financial supports from the National Natural Science Foundation of China (Grant No. 11972032, 11802303, 11772320, 11822209), the Strategic Priority Research Program of the Chinese Academy of Sciences (Grant No. XDB22040502), the Fundamental Research Funds for the Central Universities (Grant No. WK2090050045), USTC Research Funds of the Double First-Class Initiative (YD2480002004), and the Joint Fund of USTC-National Synchrotron Radiation Laboratory (KY2090000055) were gratefully acknowledged. This work was partially carried out at the USTC Center for Micro and Nanoscale Research and Fabrication.

Appendix A. Supporting information

Supplementary data associated with this article can be found in the online version at doi:10.1016/j.nanoen.2021.106071.

References

[1] Q. Wang, H.Y. Ding, X.S. Hu, X.X. Liang, M.M. Wang, Q. Liu, Z.J. Li, G.X. Sun, A dual-trigger-mode ionic hydrogel sensor for contact or contactless motion recognition, Mater. Horiz. 7 (2020) 2673–2682.
[2] H.S. Kang, S.W. Han, C. Park, S.W. Lee, H. Eoh, J. Baek, D.G. Shin, T.H. Park, J. Huh, H. Lee, D.E. Kim, D. Ryu, E.L. Thomas, W.G. Koh, C. Park, 3d touchless multiorder reflection structural color sensing display, Sci. Adv. 6 (2020), eabb5769.
[3] S.S. Thakur, S.S. Abdul, H.Y. Chiu, R.B. Roy, P.Y. Huang, S. Malwade, A. A. Nursetyo, Y.C. Li, Artificial-intelligence-based prediction of clinical events among hemodialysis patients using non-contact sensor data, Sensors 18 (2018) 2833.
[4] Y.J. Guo, S. Gao, W.J. Yue, C.W. Zhang, Y. Li, Anodized aluminum oxide-assisted low-cost flexible capacitive pressure sensors based on double-sided nanopillars by a facile fabrication method, ACS Appl. Mater. Inter. 11 (2019) 48594–48603.
[5] Q. Tang, M.H. Yeh, G.L. Liu, S.M. Li, J. Chen, Y. Bai, L. Feng, M.H. Lai, K.C. Ho, H. Y. Guo, C.G. Hu, Whirligig-inspired triboelectric nanogenerator with ultrahigh specific output as reliable portable instant power supply for personal health monitoring devices, Nano Energy 47 (2018) 74–80.
[6] A. Beutler, Strategy for a flexible and noncontact measuring process for freeforms, Opt. Eng. 55 (2016), 071206.
[7] S.C. Huang, W.H. Hsu, P.C.P. Chao, C.H. Tsai, A new active 3d optical proximity sensor array and its readout circuit, IEEE Sens. J. 14 (2014) 2185–2192.
[8] S. Qi, H.Y. Guo, J. Chen, J. Fu, C.G. Hu, M. Yu, Z.L. Wang, Magnetorheological elastomers enabled high-sensitive self-powered tribo-sensor for magnetic field detection, Nanoscale 10 (2018) 4745–4752.
[9] J. Wu, Z.X. Wu, H.J. Ding, Y.M. Wei, X. Yang, Z.Y. Li, B.R. Yang, C. Liu, L. Qiu, X. T. Wang, Multifunctional and high-sensitive sensor capable of detecting humidity, temperature, and flow stimuli using an integrated microheater, ACS Appl. Mater. Interfaces 11 (2019) 43383–43392.
[10] J.H. Yang, R.L. Shi, Z. Lou, R.Q. Choi, K. Jiang, G.Z. Shen, Flexible smart noncontact control systems with ultrasensitive humidity sensors, Small 15 (2019), 1902801.
[11] J. Ge, X. Wang, M. Drack, O. Volkov, M. Liang, G.S.C. Bermudez, R. Illing, C. A. Wang, S.Q. Zhou, J. Fassbender, M. Kaltenbrunner, D. Makarov, A bimodal soft electronic skin for tactile and touchless interaction in real time, Nat. Commun. 10 (2019) 4405.
[12] S. Niu, Y. Liu, S. Wang, L. Lin, Y.S. Zhou, Y. Hu, Z.L. Wang, Theoretical investigation and structural optimization of single-electrode triboelectric nanogenerators, Adv. Funct. Mater. 24 (2014) 3332–3340.
[13] H.M. Yang, M.M. Deng, Q. Tang, W.C. He, C.G. Hu, Y. Xi, R.C. Liu, Z.L. Wang, A nonencapsulative pendulum-like paper-based hybrid nanogenerator for energy harvesting, Adv. Energy Mater. 9 (2019), 1901149.
[14] X.J. Pu, H.Y. Guo, Q. Tang, J. Chen, L. Feng, G.L. Liu, X. Wang, Y. Xi, C.G. Hu, Z. L. Wang, Rotation sensing and gesture control of a robot joint via triboelectric quantization sensor, Nano Energy 54 (2018) 453–460.
[15] J.M. Ma, J.Q. Zhu, P. Ma, Y. Jie, Z.L. Wang, X. Cao, Fish bladder film-based triboelectric nanogenerator for noncontact position monitoring, ACS Energy Lett. 5 (2020) 3005–3011.
[16] W.L. Yin, Y.D. Xie, J. Long, P.F. Zhao, J.K. Chen, J.K. Luo, X.Z. Wang, S.R. Dong, A self-power-transmission and non-contact-reception keyboard based on a novel resonant triboelectric nanogenerator (r-teng), Nano Energy 50 (2018) 16–24.
[17] Y.J. Tang, H. Zhou, X.P. Sun, N.H. Diao, J.B. Wang, B.S. Zhang, C. Qin, E.J. Liang, Y.C. Mao, Triboelectric touch-free screen sensor for noncontact gesture recognizing, Adv. Funct. Mater. 30 (2020), 1907893.
[18] H. Wu, Z. Su, M. Shi, L. Miao, Y. Song, H. Chen, M. Han, H. Zhang, Self-powered noncontact electronic skin for motion sensing, Adv. Funct. Mater. 28 (2018), 1704641.
[19] S. Wang, S.H. Xuan, W.Q. Jiang, W.F. Jiang, L.X. Yan, Y. Mao, M. Liu, X.L. Gong, Rate-dependent and self-healing conductive shear stiffening nanocomposite: a novel safe-guarding material with force sensitivity, J. Mater. Chem. A 3 (2015) 19790–19799.
[20] C.Y. Zhao, Y.P. Wang, S.S. Cao, S.H. Xuan, W.Q. Jiang, X.L. Gong, Conductive shear thickening gel/kevlar wearable fabrics: a flexible body armor with mechano-electric coupling ballistic performance, Compos. Sci. Technol. 182 (2019), 107782.
[21] S. Wang, L. Gong, Z. Shang, L. Ding, G. Yin, W. Jiang, X. Gong, S. Xuan, Novel safeguarding tactile e-skins for monitoring human motion based on sst/pdms-agnw-pet hybrid structures, Adv. Funct. Mater. 28 (2018), 1707538.
[22] E. D'Elia, S. Barg, N. Ni, V.G. Rocha, E. Saiz, Self-healing graphene-based composites with sensing capabilities, Adv. Mater. 27 (2015) 4788–4794.
[23] C.S. Boland, U. Khan, G. Ryan, S. Barwich, R. Charifou, A. Harvey, C. Backes, Z. Li, M.S. Ferreira, M.E. Möbius, Sensitive electromechanical sensors using viscoelastic graphene-polymer nanocomposites, Science 354 (2016) 1257–1260.
[24] H. Guo, H.X. Wu, Y. Song, L.M. Miao, X.X. Chen, H.T. Chen, Z.M. Su, M.D. Han, H. X. Zhang, Self-powered digital-analog hybrid electronic skin for noncontact displacement sensing, Nano Energy 58 (2019) 121–129.
[25] Y. Liu, X.L. Shi, S.R. Liu, H.P. Li, H.L. Zhang, C.H. Wang, J.J. Liang, Y.S. Chen, Biomimetic printable nanocomposite for healable, ultrasensitive, stretchable and ultradurable strain sensor, Nano Energy 63 (2019), 103898.
[26] Y. Miwa, K. Taira, J. Kurachi, T. Udagawa, S. Kutsumizu, A gas-plastic elastomer that quickly self-heals damage with the aid of co2 gas, Nat. Commun. 10 (2019) 1828.
[27] K. Parida, G. Thangavel, G.F. Cai, X.R. Zhou, S. Park, J.Q. Xiong, P.S. Lee, Extremely stretchable and self-healing conductor based on thermoplastic elastomer for all-three-dimensional printed triboelectric nanogenerator, Nat. Commun. 10 (2019) 2158.
[28] J.N. Deng, X. Kuang, R.Y. Liu, W.B. Ding, A.C. Wang, Y.C. Lai, K. Dong, Z. Wen, Y. X. Wang, L.L. Wang, H.J. Qi, T. Zhang, Z.L. Wang, Vitrimer elastomer-based jigsaw puzzle-like healable triboelectric nanogenerator for self-powered wearable electronics, Adv. Mater. 30 (2018), 1705918.
[29] J.M. Sun, X. Pu, M.M. Liu, A.F. Yu, C.H. Du, J.Y. Zhai, W.G. Hu, Z.L. Wang, Self-healable, stretchable, transparent triboelectric nanogenerators as soft power sources, ACS Nano 12 (2018) 6147–6155.
[30] X. Cui, Y.M. Zhang, G.W. Hu, L. Zhang, Y. Zhang, Dynamical charge transfer model for high surface charge density triboelectric nanogenerators, Nano Energy 70 (2020), 104513.
[31] F. Guan, Y. Xie, H. Wu, Y. Meng, Y. Shi, M. Gao, Z. Zhang, S. Chen, Y. Chen, H. Wang, Q. Pei, Silver nanowire-bacterial cellulose composite fiber-based sensor for highly sensitive detection of pressure and proximity, ACS Nano 14 (2020) 15428–15439.